

**OPTIMIZATION STRATEGIES OF ELECTRODE
ARRAYS USED IN NUMERICAL AND FIELD 2D
RESISTIVITY IMAGING SURVEYS**

FOUZAN ALI ALFOUZAN

UNIVERSITI SAINS MALAYSIA

2008

**OPTIMIZATION STRATEGIES OF ELECTRODE ARRAYS USED IN
NUMERICAL AND FIELD 2D RESISTIVITY IMAGING SURVEYS**

by

FOUZAN ALI ALFOUZAN

**Thesis submitted in fulfillment of the requirements
for the degree of
Doctor of Philosophy**

November 2008

ACKNOWLEDGEMENTS

I would like to take this opportunity to thank every one who assisted me in finishing this thesis. First and foremost, I would like to thanks Allah the Almighty for His Most Gracious Kindness in allowing me to finish this work.

I would like to express my deep gratitude to my supervisor Assoc. Prof. Dr. Mohd Nawawi Mohd Nordin and my former supervisor who has left the university Dr. Loke Meng Heng, for introducing to me the optimization strategies and for there guidance and support during the progress of this work. Also, their encouragement, valuable advice, help and kind supervision are highly appreciated. My deep gratitude also goes to my co-supervisor, Dr. Jamhir Safani for his guide, valuable comments and great suggestions during writing my thesis.

I would like also to thank all the technical staff in the Geophysics lab for there help in both field and laboratory work during my research. My thanks go to my friend, Hussein Moussa a PhD student, for his encouragement and assistance towards my study especially during the field work.

Many thanks and highly appreciated is to the King AbdulAziz City for Science and Technology for the financial support.

My greatest thanks go to my parents for their support and encouragement from childhood, and to my wife Munirah for her support, understanding and patience. Thanks also go to my kids Reem, Noura and Ali for their understanding and patience.

TABLES OF CONTENTS

	Page	
Acknowledgements	ii	
Tables of Contents	iii	
List of Tables	viii	
List of Figures	ix	
List of Abbreviations	xvii	
List of Symbols	xviii	
Abstrak	xx	
Abstract	xxii	
CHAPTER 1 – INTRODUCTION		
1.1	Motivation	1
1.2	Techniques used in this research	2
1.2.1	2D Electrical Imaging Surveys	2
1.2.2	2D Forward Modeling	5
1.2.3	2D Inversion Method	6
1.2.4	3D Electrical Imaging Surveys	8
1.3	Conventional Array Types	10
1.3.1	Wenner Arrays	10
1.3.2	Dipole-Dipole Array	10
1.3.3	Wenner-Schlumberger	11
1.4	Optimized Strategies Configurations	12
1.5	Literature Review and Previous work	13
1.6	Objective of the Present Research Study	15
1.7	Organization of Thesis	19

CHAPTER 2 – OPTIMIZATION STRATEGIES OVERVIEW

2.1	Introduction	21
2.2	Overview of the Optimization Strategies used in this Thesis	24
2.3	Configuration Assessment using Model Resolution Estimates	26
2.3.1	Compare R Strategy	26
2.3.2	BGS Strategy	27
2.3.3	ETH Strategy	29
2.3.4	Combined BGS – CR Strategy	30
2.4	Methodology to create Optimized Strategies	30

CHAPTER 3 - MODEL RESOLUTION TESTS

3.1	Introduction	41
3.2	First Arrangement of 30 Electrodes with 1 m Spacing	41
3.2.1	Average of Relative Model Resolution R_r with Iteration number	50
3.2.2	Average of Time Consuming with Iteration number for 30 Electrodes Arrangement	51
3.3	Second Arrangement of 41 Electrodes with 1 m Spacing	52
3.3.1	Average of Relative Model Resolution R_r with Iteration Number	61
3.3.2	Average of Time Consuming with Iteration number for 41 Electrodes Arrangement	62
3.4	Third Arrangement of 61 Electrodes with 1 m Spacing	63
3.4.1	Average of Relative Model Resolution R_r with Iteration Number	71
3.4.2	Average of Time Consuming with Iteration number for 61 Electrodes Arrangement	72
3.5	Conclusion	73

CHAPTER 4 - SYNTHETIC MODEL TEST

4.1	Introduction	75
4.2	USM Synthetic Model	76
4.2.1	Forward Model of the USM Synthetic Model	76
4.2.2	Inversion Method of the USM Synthetic Data Sets	77
4.2.2(a)	Conventional arrays	77
4.2.2(b)	Optimized strategies	81
4.3	BGS Synthetic Model	83
4.3.1	Forward Model for the BGS Synthetic Model	83
4.3.2	Inversion Method of the BGS Synthetic Data Sets	84
4.3.2(a)	Conventional arrays	84
4.3.2(b)	Optimized strategies	87
4.4	Stummer Synthetic Model	90
4.4.1	Forward Model of the Stummer synthetic Model	90
4.4.2	Inversion Method of the Stummer Synthetic Data Sets	91
4.4.2(a)	Conventional arrays	91
4.4.2(b)	Optimized strategies	94
4.5	Cavities Synthetic Model	97
4.5.1	Forward Model of the Cavities Synthetic Model	97
4.5.2	Inversion Method of the Cavities Synthetic Data Sets	98
4.5.2(a)	Conventional arrays	98
4.5.2(b)	Optimized strategies	101

4.6	Saltwater Intrusion Synthetic Model	103
4.6.1	Forward Model of the Saltwater Intrusion Synthetic Model	103
4.6.2	Inversion Method of the Saltwater Intrusion Synthetic Data Sets	104
4.6.2(a)	Conventional arrays	104
4.6.2(b)	Optimized strategies	108
4.7	Conclusion	112

CHAPTER 5 - FIELD MODEL TEST

5.1	Introduction	113
5.2	The Instrument Used in the Field Work	113
5.2.1	The ABEM SAS 4000 System	113
5.3	The “USM Underground Pipe” Site, Penang Island	116
5.3.1	Introduction	116
5.3.2	Geography and Geology of the Survey Areas	116
5.3.3	Field Procedure and Results	120
5.3.3(a)	Conventional arrays	120
5.3.3(b)	Optimized strategies	124
5.4	The “Saline Water Intrusion” Site of Bertam Kepala Batas	126
5.4.1	Introduction	126
5.4.2	Geology of Bertam Kepala Batas	127
5.4.3	Interpretation of the Saltwater and Fresh Water Boundary	131
5.4.4	Results	133
5.4.4(a)	Conventional arrays	135
5.4.4(b)	Optimized strategies	138
5.5	The “Cavity” Site of Kangar, Perlis	141

5.5.1	Introduction	141
5.5.2	Geology of Kangar Area, Perlis	143
5.5.3	Preliminary Data Acquisition, Processing, and Interpretation	147
5.5.4	Results Obtained	155
5.5.5	Conclusion	165
CHAPTER 6 – CONCLUSION AND RECOMMENDATION		
6.1	Conventional Arrays	166
6.2	Optimized Strategies	168
6.3	Optimization Strategies Related to the three Tests	171
6.4	Recommendation	173
	REFERENCES	176
	APPENDIX-A	182
	APPENDIX-B	188
	APPENDIX-C	194
	APPENDIX-D	200
	APPENDIX-E	206
	APPENDIX-F	212
	APPENDIX-G	218
	APPENDIX-H	224

LIST OF TABLES

		Page
Table 3.1	Comparison between the four optimized strategies in the total time taken and the average model resolution with the three different electrode arrangements.	73
Table 4.1	Comparison of the sum of RMS difference between the Conventional arrays for the USM model.	79
Table 4.2	Comparison of the sum of RMS difference between the Optimized strategies for the USM model.	81
Table 4.3	Comparison of the sum of RMS difference between the Conventional arrays for the BGS model.	85
Table 4.4	Comparison of the sum of RMS difference between the Optimized strategies for the BGS model.	88
Table 4.5	Comparison of the sum of RMS difference between the Conventional arrays for the Stummer model.	92
Table 4.6	Comparison of the sum of RMS difference between the Optimized strategies for the Stummer model.	95
Table 4.7	Comparison of the sum of RMS difference between the Conventional arrays for the Cavities model.	99
Table 4.8	Comparison of the sum of RMS difference between the Optimized strategies for the Cavities mode.	101
Table 4.9	Comparison of the sum of RMS difference between the Conventional arrays for the saltwater intrusion model.	106
Table 4.10	Comparison of the sum of RMS difference between the Optimized strategies for the saltwater intrusion model.	110
Table 5.1	Resistivity of water and sediments (Nowroozi et al., 1999).	134
Table 5.2	Simplified borehole data of log well No. BA5 Map reference qs 744113, Geology Survey of Malaysia.	135

LIST OF FIGUERS

		Page
Figure 1.1	(a) A typical field arrangement for 2D electrical imaging survey. (b) A cell-based model used for 2D resistivity inversion (After Loke et al., 2004).	4
Figure 1.2	Figure 1.2: The three different models used in the interpretation of resistivity measurements: (a) 1D Model, (b) 2D Model and (c) 3D Model (After, Loke, 2004).	5
Figure 1.3	Roll-along techniques to survey a 10 by 10 grid with a resistivity- meter system with 50 electrodes. (a) Surveys using a 10 by 5 grid with the lines in x-direction. (b) Surveys with the lines in y-direction (After Loke, 2004).	9
Figure 1.4	Schematic diagrams of the four conventional arrays, (a) Wenner- α array, (b) Wenner- β array, (c) Dipole-Dipole array and (d) Wenner-Schlumberger array. The distance between electrodes is a, and the Dipole length factor is n, and n = 1 up to 6.	12
Figure 1.5	Map showing the three-survey areas.	19
Figure 2.1	Select the model computation option to set the optimization settings.	31
Figure 2.2	The optimaztion strategies settings option window.	32
Figure 2.3	An option to create the optimized strategey.	33
Figure 2.4	Step to save the optimized strategy in the disk file.	33
Figure 2.5	The optimized strategies files after they generated.	34
Figure 2.6	Using the SAS4000 software to create a new protocol project.	35
Figure 2.7	Open the file where the optimized strategies files saved.	35
Figure 2.8	Step to choose the protocol files wanted to run in the field.	36
Figure 2.9	Compiling the protocol file is.	37
Figure 2.10	Building the protocol file.	38
Figure 2.11	Installing the protocol to the SAS4000 instrument.	39
Figure 2.12	Downloading the protocol to the SAS4000 instrument.	39

Figure 3.1	Relative model resolutions R_r for the 30 electrodes at five different stages of the optimization process for the Compare R strategy. Each column shows the results of a different iteration, with the iteration number and number of configurations in the optimized sets increasing down the page.	43
Figure 3.2	Relative model resolutions R_r for the 30 electrodes at five different stages of the optimization process for the BGS strategy. Each column shows the results of a different iteration, with the iteration number and number of configurations in the optimized sets increasing down the page.	46
Figure 3.3	Relative model resolutions R_r for the 30 electrodes at five different stages of the optimization process for the ETH strategy. Each column shows the results of a different iteration, with the iteration number and number of configurations in the optimized sets increasing down the page.	47
Figure 3.4	Relative model resolutions R_r for the 30 electrodes at five different stages of the optimization process for the Combined BGS-CR strategy. Each column shows the results of a different iteration, with the iteration number and number of configurations in the optimized sets increasing down the page.	49
Figure 3.5	Average Relative Model Resolutions as a function of iteration for each of the four-optimization strategies at 30 electrodes arrangement.	51
Figure 3.6	Average total time taken as a function of iteration for each of the four-optimization strategies at 30 electrodes arrangement.	52
Figure 3.7	Relative model resolutions R_r for the 41 electrodes at five different stages of the optimization process for the Compare R strategy. Each column shows the results of a different iteration, with the iteration number and number of configurations in the optimized sets increasing down the page.	54
Figure 3.8	Relative model resolutions R_r for the 41 electrodes at five different stages of the optimization process for the BGS strategy. Each column shows the results of a different iteration, with the iteration number and number of configurations in the optimized sets increasing down the page.	57

Figure 3.9	Relative model resolutions R_r for the 41 electrodes at five different stages of the optimization process for the ETH strategy. Each column shows the results of a different iteration, with the iteration number and number of configurations in the optimized sets increasing down the page.	58
Figure 3.10	Relative model resolutions R_r for the 41 electrodes at five different stages of the optimization process for the Combined BGS-CR strategy. Each column shows the results of a different iteration, with the iteration number and number of configurations in the optimized sets increasing down the page.	60
Figure 3.11	Average model resolutions as a function of iteration for each of the four-optimization strategies at 41 electrodes arrangement.	62
Figure 3.12	Average total time taken as a function of iteration for each of the four-optimization strategies at 41 electrodes arrangement.	63
Figure 3.13	Relative model resolutions R_r for the 61 electrodes at five different stages of the optimization process for the Compare R strategy. Each column shows the results of a different iteration, with the iteration number and number of configurations in the optimized sets increasing down the page.	65
Figure 3.14	Relative model resolutions R_r for the 61 electrodes at five different stages of the optimization process for the BGS strategy. Each column shows the results of a different iteration, with the iteration number and number of configurations in the optimized sets increasing down the page.	68
Figure 3.15	Relative model resolutions R_r for the 61 electrodes at five different stages of the optimization process for the ETH strategy. Each column shows the results of a different iteration, with the iteration number and number of configurations in the optimized sets increasing down the page.	69
Figure 3.16	Relative model resolutions R_r for the 61 electrodes at five different stages of the optimization process for the Combined BGS-CR strategy. Each column shows the results of a different iteration, with the iteration number and number of configurations in the optimized sets increasing down the page.	70

Figure 3.17	Average model resolutions as a function of iteration for each of the four-optimization strategies at 61 electrodes arrangement.	72
Figure 3.18	Average total time taken as a function of iteration for each of the four-optimization strategies at 61 electrodes arrangement.	73
Figure 4.1	(a) The pseudosection for Wenner- α array (b) USM Synthetic Model.	76
Figure 4.2	USM inversion model resistivity sections obtained with conventional Arrays (a) Dipole-Dipole, (b) Wenner- β , (c) Wenner- α , (d) Wenner-Schlumberger. The outlines of the prisms with high resistivity value are also shown.	80
Figure 4.3	USM inversion model resistivity sections obtained with optimized Strategies (a) Compare R, (b) BGS, (c) ETH, (d) Combined BGS-CR. The outlines of the prisms with high resistivity value are also shown.	82
Figure 4.4	(a) The pseudosection for Wenner- α array (b) Wilkinson Synthetic Model.	83
Figure 4.5	BGS inversion model resistivity sections obtained with conventional Arrays (a) Wenner- α , (b) Wenner- β , (c) Dipole-Dipole, (d) Wenner-Schlumberger. The outlines of the prisms with high resistivity value are also shown.	86
Figure 4.6	BGS inversion model resistivity sections obtained with optimized Strategies (a) Compare R, (b) BGS, (c) ETH, (d) Combined BGS-CR. The outlines of the prisms with high resistivity value are also shown.	89
Figure 4.7	(a) The pseudosection for Wenner- α array (b) Stummer Synthetic Model.	90
Figure 4.8	Stummer inversion model resistivity sections obtained with conventional Arrays (a) Wenner- α , (b) Wenner- β , (c) Dipole-Dipole, (d) Wenner-Schlumberger. The outlines of the prisms with high and low resistivity values are also shown.	93
Figure 4.9	Stummer inversion model resistivity sections obtained with optimized Strategies (a) Compare R, (b) BGS, (c) ETH, (d) Combined BGS-CR. The outlines of the prisms with high and low resistivity values are also shown.	96
Figure 4.10	(a) The pseudosection for Wenner- α array (b) Two blocks with low resistivity values Synthetic Model.	97

Figure 4.11	Cavities inversion model resistivity sections obtained with conventional Arrays (a) Wenner- α , (b) Wenner- β , (c) Dipole-Dipole, (d) Wenner-Schlumberger. The outlines of the prisms with low resistivity values are also shown.	100
Figure 4.12	Cavities inversion model resistivity sections obtained with optimized Strategies (a) Compare R, (b) BGS, (c) ETH, (d) Combined BGS-CR. The outlines of the prisms with low resistivity values are also shown.	102
Figure 4.13	(a) The pseudosection for Wenner- α array (b) Saltwater Intrusions Synthetic Model.	104
Figure 4.14	Saltwater Intrusion inversion model resistivity sections obtained with conventional Arrays (a) Wenner- β , (b) Wenner- α , (c) Dipole-Dipole, (d) Wenner-Schlumberger.	107
Figure 4.15	Saltwater Intrusion inversion model resistivity sections obtained with optimized Strategies (a) Compare R, (b) BGS, (c) ETH, (d) Combined BGS-CR.	111
Figure 5.1	ABEM SAS 4000 System and accessories (www.abem.se/products/sas4000/sas4000.php).	114
Figure 5.2	Data coverage of standard Wenner CVES using two cables for roll-along with three stations (ABEM System Manual).	115
Figure 5.3	Data coverage of standard Wenner CVES using Wenner_L and Wenner_S for roll-along with three stations (ABEM System Manual).	116
Figure 5.4	Map showing the location of the USM campus (After, Wijesinghe, 2004).	118
Figure 5.5	Photograph of the survey area on USM campus - Penang.	119
Figure 5.6	Schematic diagram of the Convocation Field, USM.	119
Figure 5.7	Diagram of the underground pipe.	120
Figure 5.8	“USM Underground Pipe” Site. (a) Measured apparent resistivity pseudosection of the Wenner- α array. (b) The inversion model resistivity section.	122
Figure 5.9	“USM Underground Pipe” Site. (a) Measured apparent resistivity pseudosection of the Wenner-Schlumberger array. (b) The inversion model resistivity section.	122

Figure 5.10	“USM Underground Pipe” Site. (a) Measured apparent resistivity pseudosection of the Wenner- β array. (b) The inversion model resistivity section.	123
Figure 5.11	“USM Underground Pipe” Site. (a) Measured apparent resistivity pseudosection of the Dipole-Dipole array. (b) The inversion model resistivity section.	123
Figure 5.12	USM Underground Pipe inversion model resistivity sections obtained with optimized Strategies (a) Compare R, (b) BGS and (c) Combined BGS-CR. The outline of the expected location of the big pipe is also shown.	125
Figure 5.13	Map of the Bertam Kepala Batas survey area.	127
Figure 5.14	Photograph of the survey area on Bertam Kepala Batas.	128
Figure 5.15	Geological map of the Bertam Kepala Batas survey area (north of latitude 05 ⁰ , 31’) (After Bradford, 1972).	129
Figure 5.16	Map of the saltwater-freshwater boundary (After Wijesinghe, 2004).	132
Figure 5.17	Saline Water Intrusion inversion model resistivity sections obtained with Conventional Arrays (a) Wenner- α , (b) Wenner- β , (c) Dipole-Dipole, (d) Wenner-Schlumberger.	137
Figure 5.18	Saline Water Intrusion inversion models obtained with optimized strategies (a) Compare R, (b) BGS, (c) ETH, (d) Combined BGS-CR.	140
Figure 5.19	Index Plan, showing the Location of Kangar area, Perlis (After Jones, 1978).	142
Figure 5.20	Photograph of the survey area on Kangar, Perlis.	143
Figure 5.21	Formation of sinkholes. Examples of the soil fall into cavity due to dissolution along these zones. (a) and (b) the figures show groundwater table higher the cavity. (c) and (d) show the groundwater table is lowering. (e) Formation of sinkhole has been created due to the rapid collapse of the soil (After, Sum et al., 1996).	145
Figure 5.22	Simplified distribution map of rock formation in Perlis area. (After Jones, 1978).	146
Figure 5.23	Schematic plan of the site area. Twelve 2D electrical imaging lines with 5 m spacing between each line with 1.5 m electrode spacing. The GPR survey was conducted along the same lines.	148

Figure 5.24	The “Cavity” Site (a) measured apparent resistivity pseudosection of the Wenner- β array. (b) The inverse model resistivity section for line 1.	149
Figure 5.25	The “Cavity” Site (a) measured apparent resistivity pseudosection of the Wenner- β array. (b) The inverse model resistivity section for line 2.	149
Figure 5.26	The “Cavity” Site (a) measured apparent resistivity pseudosection of the Wenner- β array. (b) The inverse model resistivity section for line 3.	150
Figure 5.27	The “Cavity” Site (a) measured apparent resistivity pseudosection of the Wenner- β array. (b) The inverse model resistivity section for line 4.	150
Figure 5.28	The “Cavity” Site (a) measured apparent resistivity pseudosection of the Wenner- β array. (b) The inverse model resistivity section for line 5.	151
Figure 5.29	The “Cavity” Site (a) measured apparent resistivity pseudosection of the Wenner- β array. (b) The inverse model resistivity section for line 6.	151
Figure 5.30	The “Cavity” Site (a) measured apparent resistivity pseudosection of the Wenner- β array. (b) The inverse model resistivity section for line 7.	152
Figure 5.31	The “Cavity” Site (a) measured apparent resistivity pseudosection of the Wenner- β array. (b) The inverse model resistivity section for line 8.	152
Figure 5.32	The “Cavity” Site (a) measured apparent resistivity pseudosection of the Wenner- β array. (b) The inverse model resistivity section for line 9.	153
Figure 5.33	The “Cavity” Site (a) measured apparent resistivity pseudosection of the Wenner- β array. (b) The inverse model resistivity section for line 10.	153
Figure 5.34	The “Cavity” Site (a) measured apparent resistivity pseudosection of the Wenner- β array. (b) The inverse model resistivity section for line 11.	154
Figure 5.35	The “Cavity” Site (a) measured apparent resistivity pseudosection of the Wenner- β array. (b) The inverse model resistivity section for line 12.	154

Figure 5.36	The “Cavity” Site (a) measured apparent resistivity pseudosection of the Wenner- β array. (b) Calculated apparent resistivity pseudosection for line 5. (c) The inverse model resistivity section for line 5.	156
Figure 5.37	The “Cavity” Site (a) measured apparent resistivity pseudosection of the Wenner- β array. (b) Calculated apparent resistivity pseudosection for line 6. (c) The inverse model resistivity section for line 6.	157
Figure 5.38	Inverse model resistivity sections for line 6 of the Cavity Site obtained with Conventional Arrays (a) Dipole-Dipole, (b) Wenner- α , (c) Wenner- β , (d) Wenner-Schlumberger.	159
Figure 5.39	Inverse model resistivity sections for line 6 of the Cavity Site obtained with optimized Strategies (a) Compare R, (b) BGS and (c) Combined BGS-CR. The outlines of the expected cavities are also shown.	161
Figure 5.40	The 3D model obtained from the inversion of the Kangar, Perlis survey area set displayed as vertical slices through the earth.	163
Figure 5.41	The 3D model obtained from the inversion of the Kangar, Perlis survey area set displayed as horizontal slices through the earth.	164

LIST OF ABBREVIATIONS

		Page
1D	One-dimensional	1
2D	Two-dimensional	1
3D	Three-dimensional	1
ERT	electrical resistivity tomography	13
BGS	British Geological Survey	14
ETH	Eidgenossische Technische Hochschule (Swiss Federal Institute and Technology)	14
CR	Compare R	15
BGS-CR	Combined BGS-CR	15
USM	Universiti Sains Malaysia	17
OOF	Object Orientated Focussing	23
RMS	Root Mean Square	78
IP	Induced Polarization	113
CVES	Continuous Vertical Electrical Sounding	115
S	Short	115
L	Long	115
BH	Borehole	133
TDS	Total Dissolved Solid	134

LIST OF SYMBOLS

		Page
r_{i-1}	model parameters	7
$i-1$	iteration number	7
g_i	discrepancy vector	7
J	Jacobian matrix	7
P	perturbation vector	7
λ_i	damping factor	7
$C^T C$	symmetric positive definite matrix	7
C1, C2	Current electrodes	10
a	Electrode spacing	10
n	Dipole factor	10
P1, P2	Potential electrodes	10
m	meter	16
Ω_m	Ohm. Meter (unit of resistivity)	17
σ_s	standard deviation	22
\bar{S}	average sensitivity	22
Z	measurements of the survey	22
β	factor used to adjust the relative weights of the sensitivity	22
S_a	average of the weighted cumulative sensitivity	22
S_c	cumulative sensitivity of survey	22
\bar{E}	the mean survey offset	22
E_a	average of array increasing offset	22
E_c	the survey increasing offset	22
R	model resolution matrix	24

I	identity matrix	24
N	Number of electrode	25
R_b	the resolution of the base set	26
R_t	the resolution of the base set plus the test configuration	26
R_c	the model resolution of the comprehensive set	28
R_r	relative model resolution	42
P_t	true resistivity	78
P_a	calculated apparent resistivity	78
n	total number of datum points	78

PENGOPTIMUMAN STRATEGI SUSUNATUR ELEKTROD DALAM SURVEI PENGIMEJAN RESISTIVITI 2D NUMERIK DAN LAPANGAN

ABSTRAK

Tesis ini membentangkan kaedah baru untuk memilih satu set susunatur yang akan memberi maklumat sub-permukaan yang maksimum menggunakan survei pengimejan elektrik 2D untuk pengukuran empat elektrod yang terhad. Set susunatur yang optimum akan dibandingkan dengan susunatur konvensional seperti susunatur *Wenner- α* , *Wenner- β* , *Wenner-Schlumberger* dan *Dipole-Dipole*. Perbandingan dibuat menggunakan resolusi model matriks R susunatur ini, inversi data sintetik dan survei lapangan. Empat strategi penkomputeran yang berlainan dibuat perbandingan untuk menghasilkan susunatur yang optimum dari segi masa dan ketepatan. Strategi pertama dinamakan *Compare R* yang dihasilkan oleh *British Geological Survey (BGS)* yang membuat perbandingan terus dengan model resolusi matrik yang menghasilkan keputusan yang paling baik tetapi lebih perlahan. Strategi kedua dan ketiga yang dihasilkan oleh *British Geological Survey* dan oleh *Stummer et al. (ETH)* menggunakan pendekatan linear berdasarkan perubahan kepada matrik Jacobian kepada beberapa peringkat dari segi magnitud adalah lebih cepat tetapi menghasilkan keputusan yang resolusinya kurang daripada strategi pertama. Satu strategi baru yang menggabungkan strategi pertama and kedua telah dicadangkan dan diberi nama *Combined BGS-CR*. Ia menghasilkan keputusan yang hampir sama dengan strategi *Compare R* tetapi lima hingga sepuluh kali lebih pantas. Lima contoh data sintetik dibuat untuk setiap set elektrod yang optimum menggunakan model-model yang mengandungi prisma resistif. Survei lapangan termasuk pengimejan lohong, sempadan antara air masin dan air tanah dan paip bawah tanah digunakan untuk membuat perbandingan keputusan tiap-tiap strategi. Keputusan

daripada kajian strategi pengoptimuman adalah lebih baik daripada susunatur konvensional. Menggunakan konfigurasi set data strategi pengoptimuman boleh memperbaiki resolusi model survei jika dibandingkan dengan susunatur konvensional. Strategi *Compare R* dan *Combined BGS-CR* menghasilkan resolusi set data yang terbaik sebab ia menggunakan hanya satu pertiga masa komputer. Dalam tiap-tiap ujian model sintetik, keputusan yang didapati menunjukkan strategi *Compare R* dan *Combined BGS-CR* adalah terbaik dengan menghasilkan resolusi yang lebih tinggi untuk mengesan blok jika dibandingkan dengan susunatur-susunatur konvensional. Keputusan yang didapati daripada set data sintetik menunjukkan strategi *Compare R* dan *Combined BGS-CR* menghasilkan resolusi model yang terbaik jika dibandingkan dengan strategi-strategi yang lain. Di lapangan, strategi-strategi pengoptimuman menghasilkan keputusan terbaik jika dibandingkan dengan susunatur-susunatur konvensional dan strategi *Compare R* and *Combined BGS-CR* menghasilkan maklumat sub-permukaan yang lebih daripada strategi *BGS* dan *Modified ETH*. Dalam susunatur konvensional, susunatur *Wenner-Schlumberger* berkemungkinan pilihan yang lebih baik untuk keadaan tertentu seperti pengecaman jaringan paip di bawah tanah. Sementara susunatur *Wenner- β* pula adalah lebih sesuai untuk mengkaji target yang lebih kecil dan pengecaman lohong.

OPTIMIZATION STRATEGIES OF ELECTRODE ARRAYS USED IN NUMERICAL AND FIELD 2D RESISTIVITY IMAGING SURVEYS

ABSTRACT

This thesis presents new techniques to select the set of array configurations that will give the maximum amount of information of the subsurface with 2D electrical imaging surveys for a limited number of four-electrode measurements. The optimized sets of array configurations are compared with conventional arrays such as the Wenner- α , Wenner- β , Wenner-Schlumberger, and Dipole-Dipole arrays. The comparisons are made using the model resolution matrices R of these arrays, inversion of synthetic data sets as well as field surveys. Four different computational strategies to generate the optimized arrays sets are compared with regards to speed and accuracy. The first strategy which was named the Compare R developed by British Geological Survey (BGS) directly compares the model resolution matrices produces the best results but is much slower. The second and third strategies developed by British Geological Survey and by Stummer et al. (ETH) use linear approximations based on the change in the Jacobian matrix are several orders of magnitude faster but produce results that are slightly less resolution than the first strategy. A new strategy which uses a combination of the first and second strategies was introduced and called Combined BGS-CR. It produces results that are almost identical to the Compare R strategy but it is about five to ten times faster. Five examples of synthetic data are generated for each optimized set of electrodes using models containing resistive prisms. The field tests include mapping of cavities, the boundary between saline and fresh groundwater and underground pipes are used to compare the results of each strategy.

The optimized strategies results obtained in this study produced the best result compare to the conventional arrays. Using the optimized strategies configuration data sets can significantly improve the survey model resolution compared with conventional arrays. The Compare R and Combined BGS-CR strategies provided the best resolution data sets since it required only one-third the computer time. In the synthetic model test the results showed that optimized strategies obtained best results with higher resolution in term to detect and resolve the blocks in each synthetic model tests compare to the conventional arrays. In the synthetic model test the results in general showed that optimized arrays obtained best results with higher resolution in term to detect and resolve the blocks in each synthetic model tests compare to the conventional arrays. The results obtained from the synthetic data set show that the Compare R and Combined BGS-CR strategies produce the best model resolution compared to the other strategies. In the field tests, the optimized strategies showed the best results compare to the conventional arrays and the Combined BGS-CR and Compare R strategies provide more subsurface information than those from BGS and ETH strategies. In the conventional arrays, the Wenner-Schlumberger array might be a suitable choice for some situations, such as for detection of the underground-pipe network. While the Wenner- β array is more suitable for investigating small targets and the cavities detection

CHAPTER ONE

INTRODUCTION

1.1 Motivation

Recent developments in the electrical exploration methods have resulted in a lot of contributions in providing accurate subsurface information. One of the most important is the increasingly widespread use of two dimensional (2D) and three dimensional (3D) resistivity surveys (Griffiths and Barker, 1993; Ritz et al., 1999; Supper, et al., 1999; White et al., 2001; Dahlin, et al., 2002).

At the present time, the 2D surveys are the most practically economic compromise both in achieving accurate results and in limiting the survey cost (Dahlin, 1996). In many geological conditions, the 2D electrical imaging surveys can produce results that are complimentary to the information obtained from other geophysical methods. The most commonly used arrays in the 2D electrical imaging surveys are conventional arrays such as the Wenner, Schlumberger or Dipole-Dipole arrays. These arrays are often well understood in terms of their depths of investigations, lateral and vertical resolution, and signal-to-noise ratios. Generally, the Wenner and Schlumberger arrays provide good vertical resolution for horizontal structures and high signal-to-noise data. Reversely, the Dipole-Dipole and pole-Dipole arrays produce poorer vertical resolution and lower signal-to-noise ratios, but have better lateral resolution (Barker, 1979; Dahlin and Zhou, 2004). However, these conventional arrays may not be the most appropriate and effective options when the time or number of measurements given for the survey is limited, or when

an object at a specific location in very complex structure becomes the target of the survey.

The use of 2D and 3D resistivity surveys has enabled us to map complex geological structures that were not previously possible with conventional 1D resistivity surveys. With the newly introduced technical developments, equipments, automatic inversion techniques, and computer hardware such surveys can now be routinely carried out by small firms.

Two previous studies carried out by Stummer et al. (2004) and Wilkinson et al. (2006) focused on optimization strategies. These studies have not fully covered the whole area concerning the comparison between the conventional arrays (Wenner- α , Wenner- β , Wenner-Schlumberger and Dipole-Dipole) and the optimized strategies in the field test and the synthetic model test. Therefore, the present study aims to examine the reliability and effectiveness of the proposed strategy (Combined BGS-CR), which is created based on a combination between the Wilkinson et al. (2006) strategies (BGS and Compare R). The examination of the reliability and effectiveness of the Combined BGS-CR strategy will be covered by comparing this strategy with other optimized strategies and with conventional arrays in three different tests (Model resolution, Synthetic model and Field tests).

1.2 Techniques Used in This Research

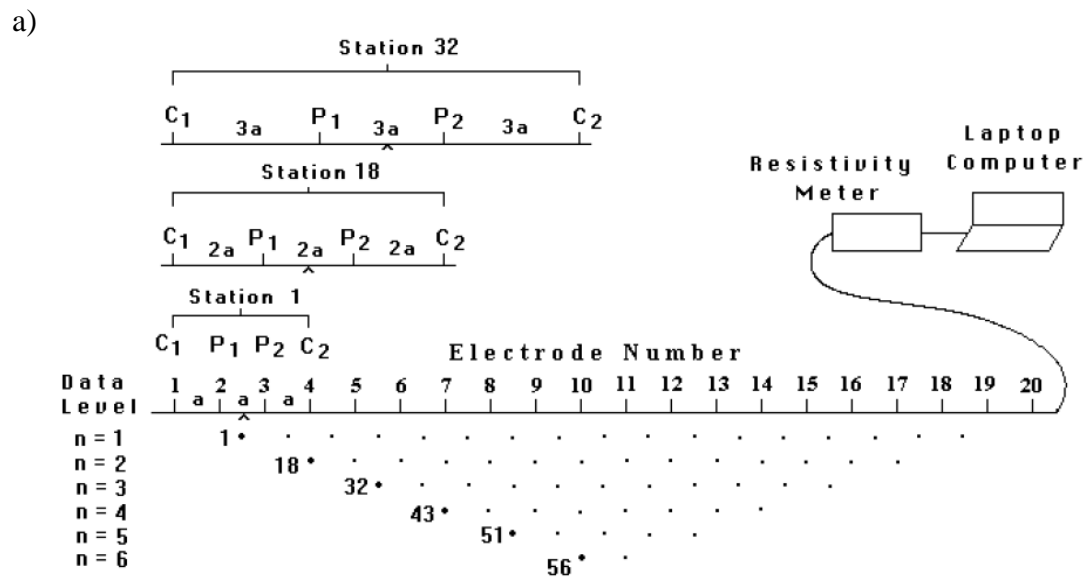
1.2.1 2D Electrical Imaging Surveys

At the present time, two dimensional 2D electrical imaging surveys (Fig. 1.1) are widely implemented for mapping areas with complex geological structures where the traditional 1D resistivity soundings surveys (which subdivides the subsurface into horizontal layers) are not sufficiently accurate (Fig. 1.2). It has become a standard

geophysical technique (Dahlin, 1996). Two dimensional electrical imaging surveys model are more accurate than 1D resistivity sounding of surveys as it allows horizontal as well as vertical resistivity variations (Loke, 2004).

Typical 1D resistivity sounding surveys usually involve approximately 10 to 20 readings, while the 2D imaging surveys contain 100 to 1000 measurements. The 2D electrical imaging method has many applications such as mapping freshwater aquifers, mapping of groundwater contamination, investigating landslides and mapping unconsolidated sediments (Acworth, 1987; Christenson and Sorensen, 1994; Barker, 1996; Johansson and Dahlin, 1996; Dahlin and Owen, 1998; Ritz et al., 1999; Nawawi et al., 2006; Umar et al., 2006).

Over the past decade, there have been many developments in instrumentation and interpretation techniques so that 2D resistivity surveys can be carried out rapidly. In addition, some research studies have shown that a number of 2D data sections can be merged into a 3D data set to produce a more accurate 3D subsurface model (Bernstone et al., 1997; Dahlin and Loke, 1997).



Sequence of measurements to build up a pseudosection

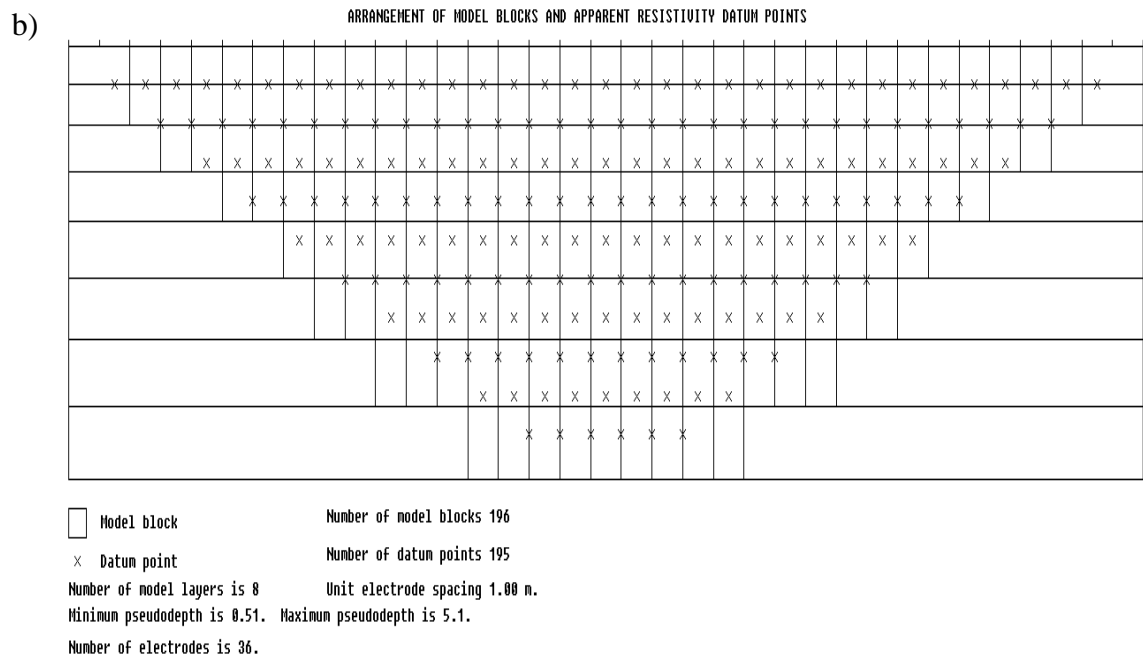


Figure 1.1: (a) A typical field arrangement for 2D electrical imaging survey.
 (b) A cell-based model used for 2D resistivity inversion (After Loke et al., 2004).

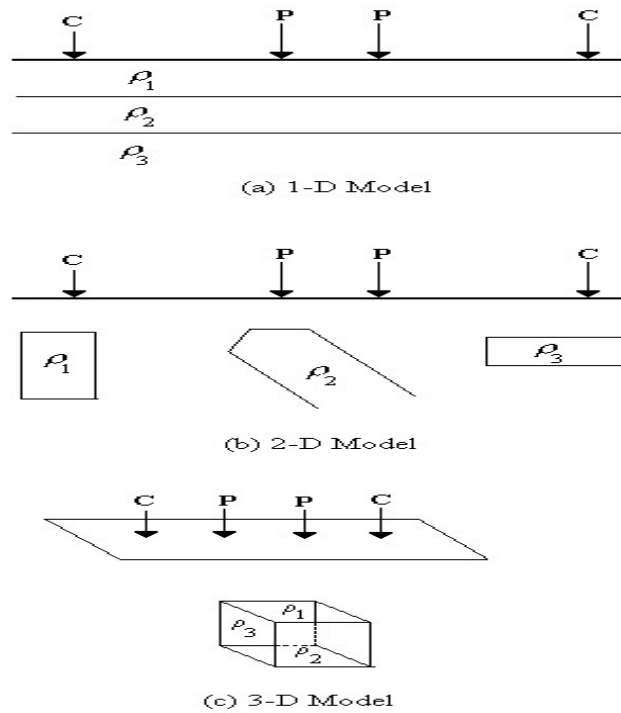


Figure 1.2: The three different models used in the interpretation of resistivity measurements: (a) 1D Model, (b) 2D Model and (c) 3D Model (After, Loke, 2004).

1.2.2 2D Forward Modeling

The forward modeling is an essential part in inversion method. It provides theoretical values for the any given model required in the inversion procedure. Three basic techniques used to evaluate the values of theoretical apparent resistivity for a defined model, respectively are; i) analytical techniques, ii) boundary element techniques, and iii) the finite-difference and finite-element techniques.

The finite-difference and finite-element techniques are normally the only practical option because in engineering and environmental surveys the subsurface can have an arbitrary distribution of resistivity. The finite-difference techniques are based on the technique described by Dey and Morrison (1979a), but with some changes by Loke (1994) to correct a minor inconsistency in the Dey and Morrison discretization by area method. The finite-element technique uses the standard first-

order triangular elements (Silvester and Ferrari, 1990). These techniques can subdivide the subsurface into thousands of cells with different values of resistivity. However, the analytical and boundary element techniques are two independent techniques that can be used to ensure the accuracy of the finite-difference and finite-element techniques (Loke, 2004).

In this research the RES2DMOD program (Loke, 2007) a modification version is used to create forward apparent resistivity values for five different synthetic models. The first forward model has two blocks. The first prism is with a resistivity value of 100 Ωm , and the second model prism has a resistivity value of 500 Ωm . Both are located at a 2 m depth near the center of the model surrounded by a 10 Ωm homogeneous medium. The two prisms represent two underground pipes with different resistivity values. One pipe with high resistivity values while the second is with low resistivity values.

The second and third models respectively are similar to the models used by Stummer et al. (2004) and Wilkinson et al. (2006), but instead of using four prisms as in Wilkinson five prisms were used. Another synthetic model has two prisms of cavities with low resistivity values of 10 Ωm located at the center of the model and at 3 m depth, and surrounded by a 100 Ωm medium which simulate cavities. The fifth synthetic model represents saltwater intrusion. This model shows low resistivity values on the left side of the model and high resistivity values on its right side with underlying bedrock at the bottom.

1.2.3 2D Inversion Method

The main objective of using the resistivity inversion in geophysics surveys is to find a desired resistivity model of the observed subsurface structures by

minimizing the misfit between the calculated and observed data. An example of the 2D inversion model is shown in Fig. 1.1b that subdivides the subsurface structure into a number of rectangular cells. The cells arrangement follows approximately the data points distribution in the apparent resistivity pseudosection. The inversion problem is to find resistivity values of the cells that have best fitness between the measured and calculated apparent resistivity values. The following equation (Ellis and Oldenburg, 1994) is used for the inversion of apparent resistivity values:

$$\left(J_i^T J_i + \lambda_i C^T C \right) P_i = J_i^T g_i - \lambda_i C^T C r_{i-1} \quad (1.1)$$

the r_{i-1} is the model parameters for the $i-1$ iteration number which is the logarithm of the model resistivity values g_i is the discrepancy vector containing the difference between the logarithms of the measured and calculated apparent resistivity values. J is the Jacobian matrix of partial derivatives, P is the perturbation vector to the model parameters, λ_i is the damping factor and $C^T C$ is a symmetric positive definite matrix (deGroot-Helding and Constable, 1990).

The damping factors depend on the inversion process. It is initially set at a large value and with each iteration the damping factor is reduced until it reaches the minimum value (Loke and Barker, 1996) which is normally set at one tenth of the initial damping factor (Loke and Dahlin, 2002). The value of the damping factor depends on the amount of random noise in the data (Sasaki et al., 1992).

To estimate the resistivity values, the apparent resistivity data are inverted using inversion modeling software of RES2DINV (Loke, 2007). The results are used to generate 2D resistivity sections which are then utilized to characterize the subsurface structures of the investigated site.

1.2.4 3D Electrical Imaging Surveys

Most geological structures are three dimensional (3D) in nature. A 3D interpretation resistivity model as shown in Fig. (1.2c) is an active area of investigation at the present time. The 3D resistivity imaging method is probably the best method to map 3D structures. But its usage is not as routinely as the 2D survey. This is because of the higher cost of a 3D survey for covering a large survey area. However, there are two recent developments that probably make 3D survey more cost-effective choice in the near future. Firstly, a multi-channel resistivity-meter which makes more than one reading at the same time can significantly reduce the survey time. The multi-electrode or multi-channel resistivity imaging systems are now readily available so many researchers are carrying out 3D resistivity surveys. Moreover, new faster microcomputers can enhance the inversion of huge data sets (Loke, 2004).

The most common way to build a 3D data set is by applying a number of 2D survey lines and then combines them into 3D data set. These lines have to be parallel to each other with constant line spacing. In the field, there have to be a set of survey lines with dimensions both in the x and y directions. Yang and Lagmanson (2006) found that to get the best 3D resistivity survey it has to use a large number of cross-line measurements with the true 3D survey because it offers a better subsurface resolution compare to the pseudo 3D survey. But even if the pseudo 3D survey run out without any cross-line measurements, it is still an acceptable choice to a true 3D survey as far as the line spacing is equal to or less than twice the electrode spacing. Therefore, in term of any project that has limited number of electrodes it can be able now to obtain a high resolution result from the 3D survey.

Loke (2004) gave an example of roll-along technique (Fig. 1.3) that used 10 by 10 grids with 50 electrodes to the resistivity-meter system. The survey shows how to collect data in both x and y directions. The advantage of measurements in two perpendicular directions is to minimize any data directional bias.

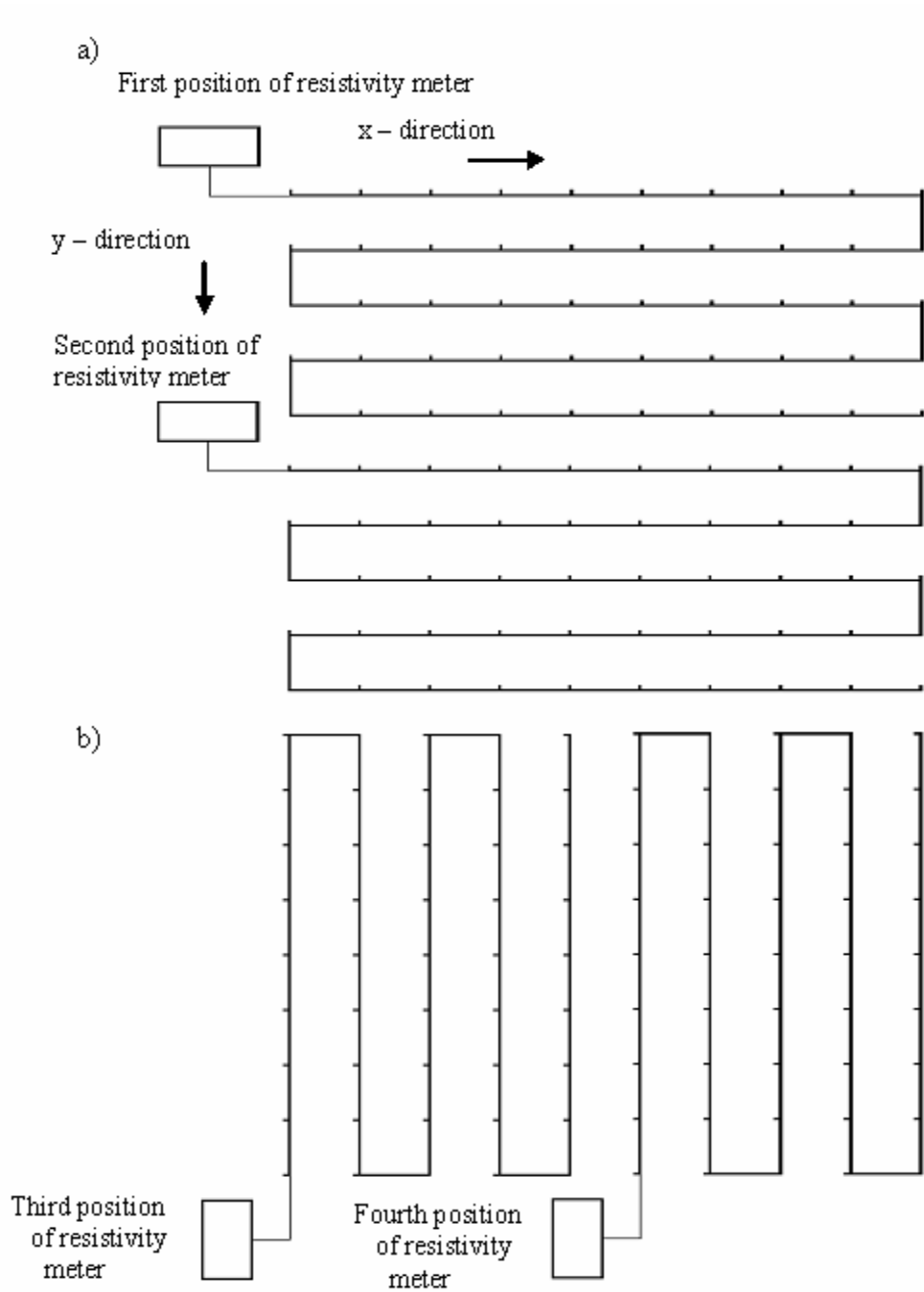


Figure 1.3: Roll-along techniques to survey a 10 by 10 grid with a resistivity- meter system with 50 electrodes. (a) Surveys using a 10 by 5 grid with the lines in x-direction. (b) Surveys with the lines in y-direction (After Loke, 2004).

1.3 Conventional Array Types

1.3.1 Wenner Arrays

The Wenner array consists of four electrodes. These electrodes are equally spaced along a survey line and the distance between adjacent electrodes is called the array spacing, a . Wenner array have three different arrangements which are referred as Wenner- α , Wenner- β and Wenner- γ . However, the Wenner- α is considered to be the standard Wenner array (Carpenter and Habberjam, 1956). The electrode arrangements of the Wenner- α and Wenner- β configurations are shown in Fig. 1.4a and 1.4b respectively. This array is used with 2D electrical imaging surveys and commonly carried out with both resistivity sounding and profiling surveys. The great advantage of this array is the ability to resolve the horizontal structure since this array is relatively sensitive to vertical resistivity changes in the subsurface structures below the center of the array. Also this array has the strongest signal strength which is an important factor at the survey area with high background noise.

On the other hand, this array is the less sensitive to horizontal resistivity changes in the subsurface structures so the disadvantage of using this array is the poor detection of the vertical structure. Also the coverage is quite poor for the horizontal direction as the electrode spacing is increased (Loke, 2004).

1.3.2 Dipole-Dipole Array

Dipole-Dipole array is mainly used in resistivity profiling and IP surveys. This array is now widely used because of the low EM coupling between the current and potential circuits (Loke, 2004). The electrode arrangements of this array are shown in Fig. 1.4c. The space between the current electrodes pair, C2-C1, and potential electrodes pair, P1-P2, is the same and specified as “ a ” Fig. 1.4c. There is

another factor used in this array named “n” which represent the ratio of the distance between the C1 and P1 electrodes to the C1-C2 (or P1-P2) Dipole length “a” (Fig. 1.4c). In order to increase the depth of the investigation in the survey the “a” spacing is to begin with constant smallest unit electrode spacing and the “n” factor is increased from 1 to 6. Then the “a” spacing is increased to “2a” and another measurement is made for the same “n” values. The process can be repeated for other “a” values (Loke, 2004).

1.3.3 Wenner-Schlumberger

This array is a combination of the Wenner and Schlumberger configurations (Pazdirek and Blaha, 1996) and become one of the important array used in the electrical imaging surveys. The Schlumberger array is commonly used for resistivity sounding surveys and the arrangement of the electrodes is shown in Fig. 1.4d. This array has better horizontal coverage compared to Wenner array.

The electrode layout in the Wenner - Schlumberger configuration, for the first datum level ($n = 1$) is the same as the Wenner array. But the “n” value for this array is the ratio of the distance between the C1-P1 (or P2-C2) electrodes to the spacing between the P1-P2 potential pair. The technique of this array during the survey uses fixed potential electrode spacing while the spacing between current electrodes is gradually increased for several Dipole lengths. Then in order to obtain more depth penetration the spacing between potential electrodes is increased (Loke, 2004).

1.4 Optimized Strategies Configurations

The configurations of all optimized strategies arrangements are discussed in Chapter 2 page 24. Also Appendix E, F, G and H are presented all configurations in details.

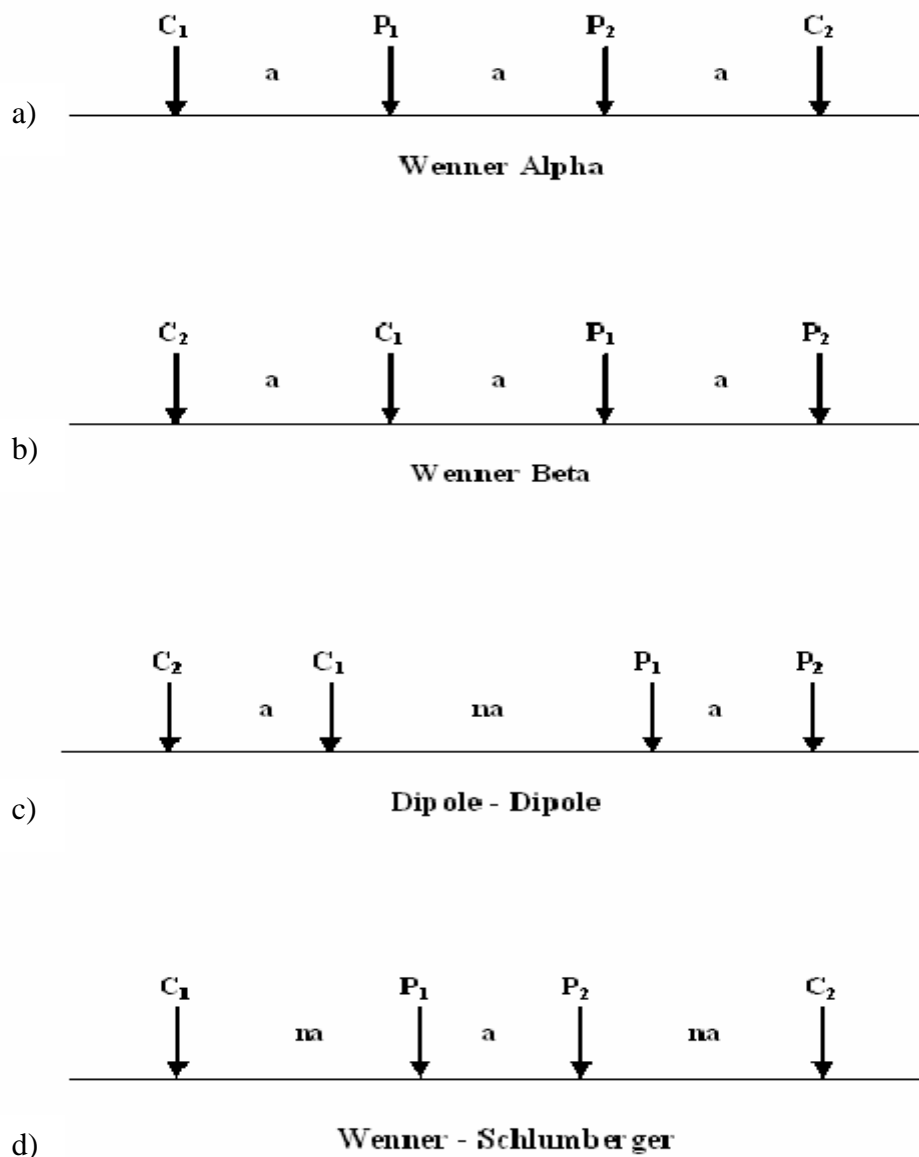


Figure 1.4: Schematic diagrams of the four conventional arrays, (a) Wenner- α array, (b) Wenner- β array, (c) Dipole-Dipole array and (d) Wenner-Schlumberger array. The distance between electrodes is a , and the Dipole length factor is n , and $n = 1$ up to 6.

1.5 Literature Review and Previous work

There have been many significant developments in the electrical exploration methods over the past decade. Despite the flexible nature of modern survey systems, resistivity surveys still commonly use conventional electrodes arrangements, such as Wenner, Schlumberger and Dipole-Dipole arrays. However, the conventional arrays may not be the most appropriate and effective options if the survey time or number of measurements given for the survey is limited, or a marked object of specific interest is spatially localized.

Therefore, at the present time, there is much interest in producing sets of electrodes configurations that optimize the resolution of the tomography image for a given number of measurements or for a particular survey region. The first attempt for data optimization implemented for resistivity imaging was made in the biomedical sciences (Isaacson, 1986). It included the adjustment of the intensity distribution of injected currents to increase the response of a marked object. The first attempt to apply data optimization in geological surveying was made by Cherkaeva and Tripp (1996), who implemented a weighted sum of pole-pole configurations to current distribution on features at specified depths and locations. Most electrical resistivity tomography (ERT) systems however allow most two currents electrodes to be implemented at a single time.

Two more methods of data optimization that are suitable to be used with multi-electrode systems have been introduced (Furman et al., 2004; Henning & Weller, 2005). Both of the methods depend on optimizing the sensitivity of the arrays to resolve separate localized resistivity variations. The sensitivity distributions are calculated analytically from the Jacobian matrix elements derived in the forward modelling step (Furman et al., 2004; Henning & Weller, 2005). Data

optimization takes place by achieving weighted sums of these distributions that increase the sensitivity either evenly across the subsurface or within localized regions. Calculating the sensitivity distributions have a perceptive appeal to model regions with high average sensitivity tended to be well resolved (Wilkinson et al., 2006).

However, it could only produce an accurate representation of subsurface resolution in limited situations. As an example when the minimal overlap between the sensitivity distributions of different arrays and the regularization restrictions are small. Stummer et al. (2004) pioneered a more quantitative approach that uses the sensitivity distributions to calculate an estimate of the resolution matrix of the model. This gives a measure of how well the observed apparent resistivity data can resolve each model cell. This optimization algorithm generated sets of electrodes configurations that out-performed conventional arrays (Wilkinson et al., 2006).

More recently, Wilkinson et al. (2006) proposed two new ERT optimization strategies which are British Geological Survey (BGS) and Compare R. Both strategies are based on finding a restricted number of electrodes configurations that improve the resolution matrix of the model. Of the two, the algorithms performed better in terms of optimizing the resolution or reducing computing time. One strategy uses approximations to maximize its speed, but manages to obtain almost optimal results. These strategies were compared with that proposed by Stummer et al. (2004) in the Eidgenossische Technische Hochschule (ETH) (Swiss Federal Institute and Technology) in terms of both performance and speed. The efficiency of the algorithms in optimizing the model resolution was compared. The results were also tested by using synthetic data for different numerical models.

1.5 Objective of the Present Research Study

The primary objective of this thesis is to present a new optimized strategy named Combined BGS-CR. This new Combined BGS-CR strategy (Loke et al., 2007) uses a combination of the two strategies of Compare R and BGS proposed by Wilkinson et al. (2006) to select the set of arrays configurations that will give the maximum amount of information about the subsurface with a 2D electrical imaging survey with a limited number of measurements. However, for clearer comparison, not only the results from this optimized strategy will be presented in this thesis, but also the results from other optimized strategies, involving the Compare R, BGS, and the ETH strategies. Their comparisons to conventional arrangements such as the Wenner- α , Wenner- β , Wenner-Schlumberger, and Dipole-Dipole arrays will also be discussed. The comparisons involve model resolution matrices, the inversion results of different synthetic data sets and as well as field data.

Four different computational strategies were used to generate the optimized arrays sets through modification version of the RES2DMOD software (Loke, 2007) that were compared with regards to their speed and accuracy. The first strategy that is the Compare R strategy was developed by Wilkinson et al. (2006) which directly calculates the model resolution matrices. The second strategy is British Geological Survey (BGS) strategy developed by Wilkinson et al. (2006), and then called as BGS strategy. The third strategy was Modified and produced by Stummer et al. (2004) from Eidgenossische Technische Hochschule (ETH), and then called as ETH strategy. Both these strategies use linear approximations based on the change in the Jacobian matrix.

The new Combined BGS-CR strategy (Loke et al., 2007) uses a combination of the first and the second type of strategies (Compare R and BGS respectively).

This strategy starts with searching for the optimal configurations using the BGS strategy and then shifts to several iterations of the Compare R strategy (which is using approximately 20% of the total iterations). It produces results that are almost identical to the Compare R strategy but is about five to ten times faster.

In this connection, the present research study aims at achieving the following objectives:

1. To examine whether the Combined BGS-CR strategy has the better model resolution and more efficient compared to other optimized strategies. The efficiency will be evaluated from the computing time used.
2. To check the reliability and effectiveness of the proposed strategy (Combined BGS-CR) that will be inspected from the model resolution matrices resulted and the inversion results of synthetic data sets as well as field data.
3. To check and compare the ability of the optimized strategies in resolving the cavity, saltwater intrusion and mapping the underground pipe.

Three different types of model resolution tests have been used for a homogeneous half-space which increased the speed and simplicity of the sensitivity calculations. The first arrangement consists of a 30 electrodes positioned at 1 m spacing, the second model resolution test configuration consists of 41 electrodes with 1 m spacing and the third example consists of 61 electrodes also with 1 m spacing.

Based on that, five types of synthetic data are generated for each optimized set of electrodes using models containing resistive prisms. These five synthetic data

sets were created and computed by using the RES2DMOD software. The first one (the Universiti Sains Malaysia (USM) synthetic model) has two resistive prisms at depth of 2 m in a background with $\rho = 10 \Omega\text{m}$. This synthetic model is based on a 41 electrodes spread with 0.5 m electrode spacing so the total length is 20 m.

The second synthetic model is similar to the Wilkinson et al. (2006) synthetic model. But It consists of five resistive prisms instead of four at Wilkinson model buried at different depths in a background with $\rho = 10 \Omega\text{m}$. This synthetic model has 41 electrodes spread with 1 m electrode spacing with total length of 40 m.

The third synthetic model is the same as the synthetic model used by Stummer et al. (2004). It has a thin surface layer with $100 \Omega\text{m}$ and an underlying layer with $\rho = 1000 \Omega\text{m}$. At a depth of 6 m on the left side of the model, there is a conductive prism with a minimum resistivity of $10 \Omega\text{m}$. This synthetic model has a 30 electrodes spread with 1 m electrode spacing with total length of 30 m. Transecting the boundary between the two layers on the right side is a $10,000 \Omega\text{m}$ resistivity prism.

The fourth synthetic model depicts cavities structures represented by two blocks of low resistivity values of $10 \Omega\text{m}$ at the center of the model and at depth of 3 m surrounded by a $100 \Omega\text{m}$ medium. This synthetic model is based on a 41 electrodes spread with 1.5 m electrode spacing so the total length is 60 m.

The fifth synthetic model represents saltwater intrusion. The low resistivity value of $5 \Omega\text{m}$ on the left side of the model represents the saline water zone at the depth of 8 m. The upper layer on the right side of the model with resistivity value of $30 \Omega\text{m}$ represents the freshwater zone. Between these zones there is a transition zone with a resistivity value of $15 \Omega\text{m}$. In addition there is another subsurface layer with a resistivity value of $200 \Omega\text{m}$ that represents bedrock at a certain depth level.

This synthetic data was computed for a data set with 41 electrodes with an electrode spacing of 10m, giving a profile length of 400m.

The field tests involve mapping of underground pipes, the boundary between saline and fresh groundwater, and mapping of cavities. The convocation area in the Universiti Sains Malaysia (USM) campus, Penang Island was chosen (Fig. 1.5) to map the underground pipe and it is located on N 05° 21' 352" and E 100° 18' 158". The geology of this area is well known based on the sewage network and the available underground pipe map. The diameter of the pipe is 0.2 meter and buried at a depth of 0.6 meter. Nearby outcrops show that the subsurface is composed of two main layers (Wijesinghe, 2004).

The Bertam Kepala Batas area located 30 km north of Penang Island was chosen as second area for detection of the saline water intrusion. The study area is located on N 50° 31' 04.5" and E 100° 27' 35.6" (Fig. 1.5). The survey line runs near the boundary between the saline and fresh water zones.

The third area for the cavity mapping is in the Kangar area of Perlis. This area is located in the northwestern region of Peninsula Malaysia about 180 km from Penang. The location of the study area is in the Bintong Primary School (Sekolah Bintong Kebangsaan) in the Kangar area, Perlis with coordinates of N 60° 26' 33.5" and E 100° 10' 11.1" (Fig. 1.5). The topography of Perlis state varies from flat coastal plains to rugged hills of almost 915 meters in height. The structure and lithology of the underlying rock very much controls the landscape. However, the Kangar area is underlain by limestone bedrock. Cavities are often found in the bedrock, buried under alluvium (Sum et al., 1996).

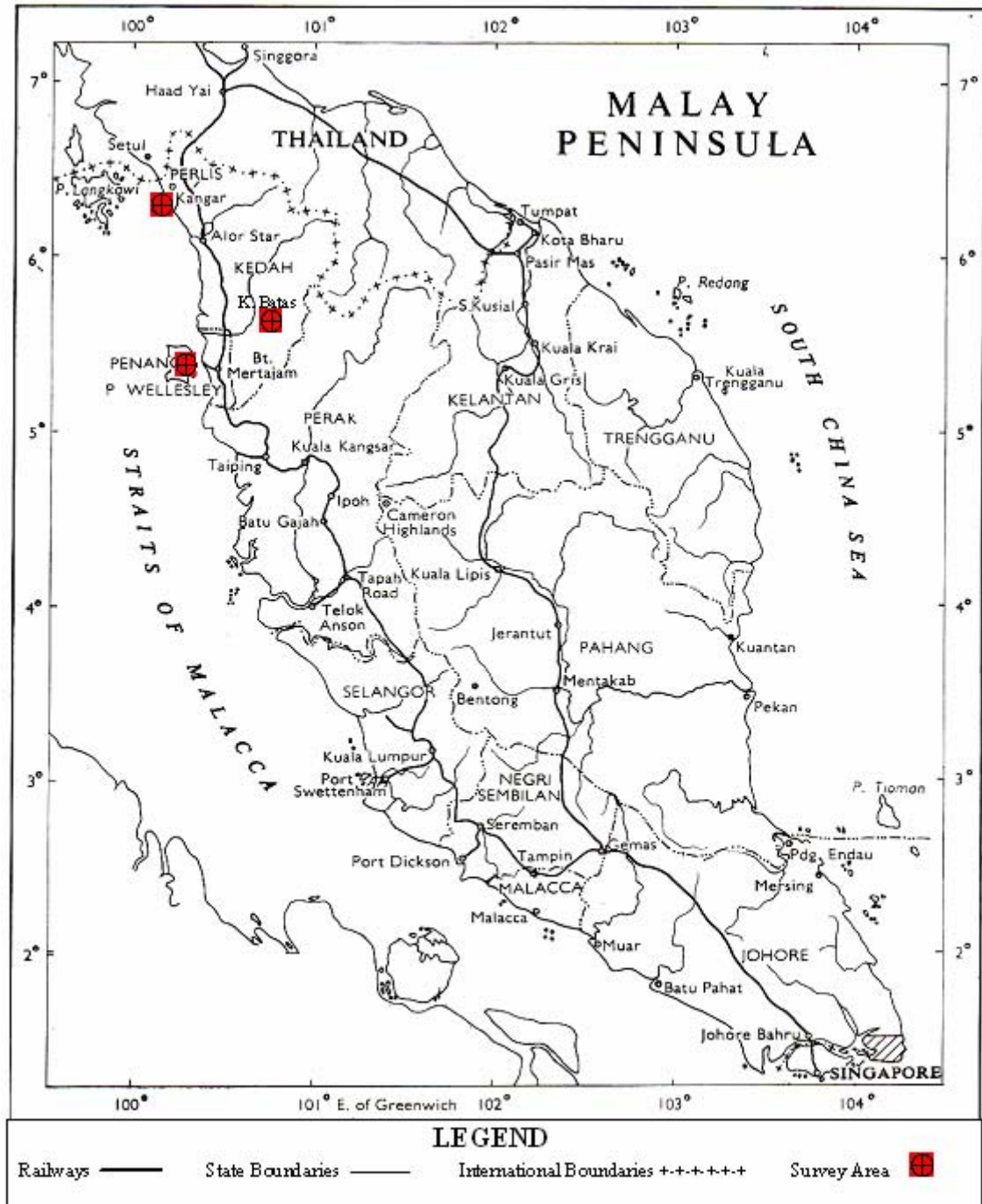


Figure 1.5: Map showing the three-survey areas.

1.6 Organization of Thesis

This thesis presents results with different techniques to select the set of optimal strategies configurations. A new strategy was compared with other

optimization strategies. The optimized sets of strategies configurations are compared with the conventional arrays such as the Wenner- α , Wenner- β , Wenner-Schlumberger, and Dipole-Dipole arrays.

This thesis starts with the background study that also contains information about the new strategy. In addition, this chapter covers previous works that have been done in this field. Chapter 2 gives some overview of each optimized strategy with some of attempt from researchers done in this field.

In Chapter 3, comparisons are carried out using the model resolution matrices of these strategies to assess the different configurations.

Chapter 4 discusses the inversion of synthetic data sets while Chapter 5 covers field surveys with the modeling examples illustrated within this chapter. The conclusions and recommendations are covered in Chapter 6. The end of this chapter gave some recommendations and implications obtained from this research.

CHAPTER TWO

OPTIMIZATION STRATEGIES OVERVIEW

2.1 Introduction

As mentioned earlier in the literature review section that many researchers have done many attempts for data optimization implemented for electrical resistivity imaging and other field too. Isaacson (1986) was the first researcher who used the resistivity imaging in the biomedical sciences that included the adjustment of the intensity distribution of injected currents to increase the response of a marked object. Mainly electrical resistivity tomography (ERT) system has the ability to implement two currents electrodes at a single time.

However, the first attempt to apply resistivity data optimization in geological surveying was made by Cherkaeva and Tripp (1996), who applied a system of pole-pole configurations to current distribution on features at particular depths and locations. They applied theoretical works into geological setting. The study showed how the numerical experiments could discover optimal perturbations determined from priori model. Therefore, they concluded that the optimal method can be used as imaging technique based on either two applications. One application is for calculating the impedance matrices by using the suitable forward algorithm model to find the corresponding currents numerically. While the second application is considered to have insufficient information of the inclusion, so it could use the measured impedance matrix then find the optimal intensity distribution over the electrodes (Cherkaeva and Tripp, 1996).

Two more methods of data optimization that are suitable to be used with multielectrode systems have been introduced by Furman et al. (2004) and Henning &

Weller (2005). Both methods depend on optimizing the sensitivity of the arrays to resolve separate localized resistivity variations. The sensitivity distributions are calculated analytically from the elements of Jacobian matrix derived in the forward modelling step.

Furman et al. (2004) designed an optimization technique to achieve as much information of the cumulative sensitivity of the arrays used in the survey. The approach produced uses the minimum value of the standard deviation σ_s of the sensitivity values. From the standard deviation and the average sensitivity \bar{S} , the measurements of the survey Z can be obtained based on these two components. Therefore to measure the objective function, the measurements of survey Z is arranged to a maximum value as following equation

$$\text{MAX}(Z) = \beta \bar{S} - (1 - \beta) \sigma_s \quad (2.1)$$

where β is a factor used to adjust the relative weights of the sensitivity. The survey sensitivity \bar{S} is the average of the weighted cumulative sensitivity S_a and the cumulative sensitivity of survey S_c . Furman et al. (2004) used the mean survey offset \bar{E} , the average of array increasing offset E_a and the survey increasing offset E_c , to change the quantity \bar{S} in the Equation (2.1) above, and gave a new formula as follows:

$$\text{MAX}(Z) = 1 - [\beta \bar{E} - (1 - \beta) \sigma_E] \quad (2.2)$$

So Furman et al. (2004) concluded that, equation (2.3) can be used to calculate the objective function considering the standard deviation of the offset as omitted when assuming that the offset is a normalized measure

$$\text{MAX (Z)} = 1 - \bar{\text{E}} \quad (2.3)$$

However, it was clearly noticed in Furman method that, some considerations should be taken into account for the effects of the inversion process including the diversity of arrays and the methods of expressing the diversity of arrays. Therefore the inversion process was effected from not taking attention to some of these factors which is require to obtain a stable and accurate inversion model an additional measure of the independence of the arrays included in a survey (Wang , 2002).

Henning and Weller (2005) also developed a method, namely Object Orientated Focussing (OOF) that concentrated only in the weighting factor. The goal of this method is to try to reduce automatically the number of electrical measurements by an optimization of the result sensitivity distribution compared to the initial sensitivity distribution. Of course with having some background about the survey area this method can be used to reduce the time of the survey by reducing the number of the electrical measurements.

Therefore both of Furman et al. (2004) and Henning and Weller (2005) methods attempted to optimize data by achieving weighted sums of these distributions that increases the sensitivity either evenly across the subsurface or within localized regions.

2.2 Overview of the Optimization Strategies used in this Thesis

All the optimization strategies discussed in this thesis depend on the assessment of the model resolution matrix \mathbf{R} . Every resistivity cell quantified degree in the model can be determined in the observed data. It is described by $\mathbf{m}^{\text{fit}} = \mathbf{R}\mathbf{m}^{\text{true}}$, where \mathbf{m}^{fit} is the model resistivity estimate decided by the process of inversion, and \mathbf{m}^{true} contains the true resistivities that are unidentified (Menke, 1984). Every row of \mathbf{R} is the restricted least-square best fit to the corresponding row of \mathbf{I} (\mathbf{I} is the identity matrix) if each model cell is completely determined then $\mathbf{R} = \mathbf{I}$ (Jackson, 1972). According to Friedel (2003), the model resolution matrix \mathbf{R} can merely be described for linear inverse problems (Wilkinson et al., 2006).

$$\left(G^T G + C \right) \Delta r_i = G^T g - Cr_{i-1} \quad (2.4)$$

The Jacobian matrix component \mathbf{G}_{ij} is the logarithmic sensitivity of the i -th measurement to a small modification in the resistivity of the j -th model cell, and \mathbf{C} comprises the damping factors, constrains and spatial filters that restricts the inversion (Loke et al., 2003). While \mathbf{g} is the data misfit vector containing the difference between the logarithms of the measured and calculated apparent resistivity values (Loke et al., 2003). The quantity \mathbf{r}_{i-1} is the model parameter vector (the logarithm of the model resistivity values) for the previous iteration, while $\Delta \mathbf{r}_i$ is changed in the model parameters (Loke et al., 2007).

Therefore, the inversion of ERT is implemented through linearized steps iterative series considering that, the forward problem is non-linear (Loke & Barker, 1995). As a result, the estimate of the model resolution matrix can be described as: